Korean Journal of Cosmetic Science
Vol. 2, No. 1, December 2020, 33-46

pISSN 2713-5411
http://dx.doi.org/10.15230/SCSK.2020.2.1.33

Effects of Linear and Nonlinear Shear Deformation on Measurement for Stickiness of Cosmetics Using Rotational Rheometer

Jung-Eun Bae†, Joo-Yeon Ryoo, and Nae-Gyu Kang

LG Household & Health Care, E10 LG Science Park, 70 Magokjungang 10-ro, Gangseo-gu, Seoul 07795, Korea
(Received June 12, 2020; Revised August 4, 2020; Accepted August 26, 2020)

Abstract: Cosmetics are representative complex fluids, and there have been many studies focusing on the correlation between the rheological properties and sensory attributes. Various instrumental measurements have been suggested to evaluate the sensory attributes, and one of the most common instruments is Texture Analyzer (TA). Although it is reported that the adhesiveness measured by TA is related to the stickiness of cosmetics, there exists reproducibility problem because measurements with TA are sensitive to application conditions. In this study, an instrumental protocol using rotational rheometer has been set up to measure the stickiness of cosmetics. This protocol consists of two steps. The first step is a preconditioning step, and various types of shear deformations are applied to the samples. The next step is the extensional flow and the axial force is measured. When the amplitude of the shear flow corresponded to the linear viscoelastic region, the axial force is the same as those without preconditioning. On the other hand, an axial force decreases as variation nonlinearity increases. It is because the effects of microstructure changes caused by nonlinear deformation affects the extensional flow. It is worth noting that a new protocol facilitates to evaluate the stickiness of cosmetics in a more systematic way.

Keywords: stickiness, rotational rheometer, axial force, small amplitude oscillatory shear, large amplitude oscillatory shear

1. Introduction

There have been lots of attempts to characterize the textural properties of cosmetic products using mechanical measurements. Since, especially as for the cosmetic products, texture is closely related to the sensory assessment, many researchers have tried to find the relation between the qualitative sensory properties and quantitative values. The most widely used method is a panel test. The panel test provides numerous information for the skin feel as well as preferences. However, it always suffers from the interference of personality of subjects. Indeed, the most of panel test in terms of general consumers performed the test based on their experiences[1].

Many researchers have focused on tribology as a key factor determining sensorial properties[2-5]. According to their studies, the friction coefficient plays an important role to control the softness of the solid surface. They tried to find the relation between the friction coefficients of surface covered by cosmetic products and sensory assessments obtained by panel tests. Timm et al. found that the cosmetic powder particles should be small with an irregular shape to enhance the "powdery" skin feel for simple formulation cosmetic products[2]. It was reported that the tribology can be related to the application, but not for initial skin feel. It is because that the methods used for friction are more suitable for characterizing solid-like surfaces than liquid-like surfaces[3].

Texture analyzer (TA) has been spotlighted as a useful tool to measure the mechanical properties which is related to the texture characteristics in the cosmetic industry as well as in the food industry[6,7]. Various probes can be equipped by simple operation and the experimental sequence can be designed by vertical movement of the upper

† Jung-Eun Bae (e-mail: jungeunbae@lghnh.com), call: 02-6980-1517

probe. However, it strongly depends on the loading condition of samples. In order to simulate the skin feel coated by the cosmetic products, various researchers introduced TA, but it was affected by the experimenter who spread the samples on the substrate surface[8]. Compared with the previous instruments mentioned above, the rotational rheometer can control the shear flow with high sensitivity by the advanced torque motor[9]. There were many researcher who tried to relate the rheological behavior and the textural performance of viscoelastic materials[10-12]. These studies mainly focused on rheological variables measured by various flows and attempted to find correlations with panel tests scores through statistical processing[13].

The stickiness is one of the major factors determining the quality of cosmetic products. It was expected that the stickiness could be explained by the adhesion properties due to the microstructural differences[14-18]. Recently, Eudier et al. suggested the new method to measure the stickiness of various cosmetic products such as hair gel, face care cream and hand cream. They compared the adhesion energy using TA equipped the spherical steel on the surface of human skin, artificial skin and resin sheets. It was found that the adhesion energy in logarithmic scale represents the stickiness obtained by sensory assessments. However, it is still remains discrepancies comes from the difference of skins according to ages, hardness of arm and skin temperature. Most of all, it is hard to control the residual film thickness and amount because it strongly depends on an experimenter[8].

This study aimed to suggest an effective method to measure the axial force using the rotational rheometer, focusing on the effects of preconditioning shear flows on axial forces under the extensional flow of cosmetics. The preconditioning step was controlled by 4 types of flow: (1) static state (2) step shear with constant shear rate (3) linear and (4) nonlinear oscillatory shear flow. Fourier transform (FT) rheology was adopted to analyze linear and nonlinear viscoelastic response under oscillatory shear flow. The effects of preconditioning shear flow on axial forces were observed based on nonlinear parameters derived from FT rheology. Measurements using TA and panel test were performed and the availability of the new protocol was confirmed against the axial forces measured by the rotational tachometer.

2. Theoretical Background

Oscillatory shear flow is a useful tool for characterizing viscoelastic fluids because it is governed by the frequency and amplitude of oscillatory stimulus. It also ensures more stable and reproducible data compared to the step shear or elongational flows. When the amplitude of oscillatory shear flow is small so that the relation between the input and output signal represents a linear relation, this is called the small amplitude oscillatory shear (SAOS) test. If the amplitude of the stimulus is sufficiently large to cause a nonlinear response, this is called large amplitude oscillatory shear (LAOS) flow. LAOS has been spotlighted as a useful tool for studying nonlinear behavior since it can easily control flow conditions compared to extensional or capillary rheometer[19-20].

Early studies on LAOS mainly used qualitative analysis methods to analyze nonlinear behavior of LAOS flow. When the amplitude of the oscillation stimulus falls within the SAOS region, the stress or strain response shows a sinusoidal waveform shifted horizontally with a phase angle, δ on the time scale. However, as the strain or stress amplitude of the stimulus increases, the response curve begins to distort in the sine wave. This phenomenon is more apparent when plotted as a strain stress plot rather than a waveform as a function of time. It is referred to as the Lissajous–Bowditch plot[21-23].

Because of its simplicity, the Lissajous–Bowditch plot has been widely used to study the nonlinear viscoelastic behavior under LAOS[24, 25]. The Pipkin diagram was used since it showed the Lissajous plots of the oscillating shear for various strain (or stress) amplitude and frequency conditions at a glance[26]. The occurrence of secondary loops in Lissajous–Bowditch plot has been reported as results of instability under severe condition of LAOS or effects of branching in polymer melts[27,28]. Cho et al. adopted the 3–dimensional Lissajous–Bowditch plot to in-

vestigate the nonlinear behavior in the plane of shear stress–strain as well as stress–strain rate[29]. It enhances the quality of the qualitative investigation for nonlinear viscoelastic behavior under LAOS[30,31].

While the early stages of research for LAOS focused on qualitative perspectives, efforts have been made to quantitatively analyze nonlinear viscoelastic behavior. FT rheology is one of the most popular methods[32-34]. When the induced deformation is written as below

$$\gamma(t) = \gamma_0 \sin(\varpi t) \tag{1}$$

in linear viscoelastic region, shear stress is observed as

$$\sigma(t) = \sigma_0 \sin(\varpi t + \delta) \tag{2}$$

The storage and loss moduli can be defined by simple relation between shear stress and strain under SAOS flow as follow.

$$\sigma(t) = G'(\varpi)\gamma(t) + G''(\varpi)\frac{1}{\varpi}\frac{d\gamma(t)}{dt} \tag{3}$$

where

$$G'(\varpi) = \frac{\sigma_o}{\gamma_o}\cos\delta(\varpi);\ G''(\varpi) = \frac{\sigma_o}{\gamma_o}\sin\delta(\varpi) \tag{4}$$

and δ means the phase difference between the input and output signals. When the strain amplitude does not belong in linear viscoelastic region, additional harmonic terms are needed to express the response stress as follows:

$$\sigma(t;\gamma_o,\omega) = \sum_{k=0}^{\infty} I_{2k+1}\sin[(2k+1)\varpi t + \delta_{2k+1}] \tag{5}$$

When only the first term with k = 0 exists, Equation (5) can express shear stress in the linear viscoelastic region like Equation (2). As nonlinearity increases, the Fourier intensities of the higher harmonics increased. In most cases, the relative intensity normalized to the linear viscoelastic variable is used to indicate the relative nonlinearity to the linear viscoelasticity.

Figure 1 shows the linear and nonlinear waveforms analyzed by qualitative and quantitative methods, which are obtained in response to a sinusoidal input signal. In order

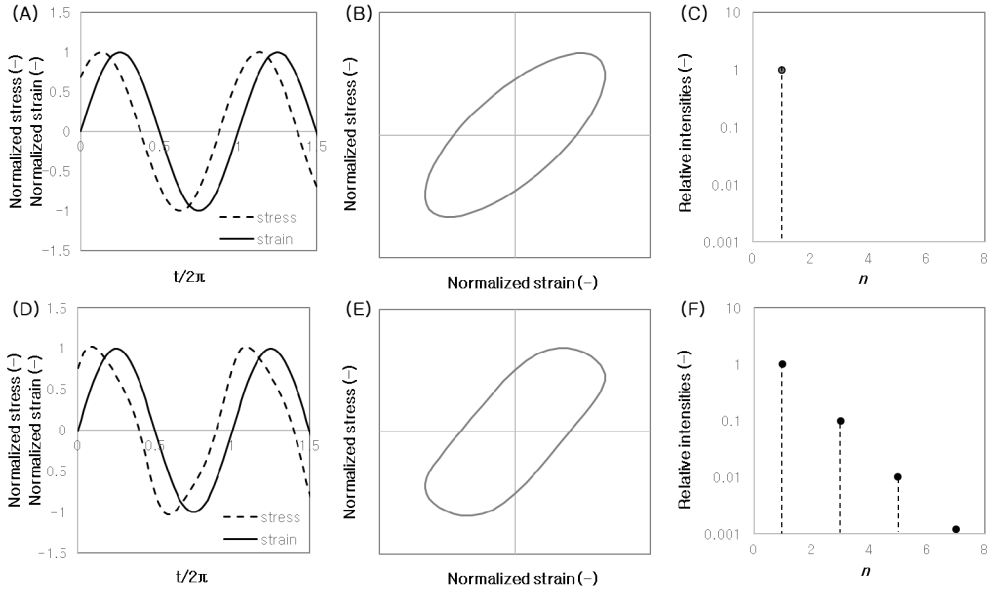

Figure 1. Linear and nonlinear responses to the sinusoidal input stress. (A) sinusoidal input stress and output strain; (B) Lissajous–Bowditch plot of (A); (C) Fourier intensities of (A); (D) non-sinusoidal strain response to the sinusoidal input stress; (E) Lissajous–Bowditch plot of (D); (F) Fourier intensities of (D).

to clarify the shape of the curves, strain and stress curves are normalized by the maximum values of each curve. As shown in Figure 1A, when stimulus is given as a sine function, those amplitude are in linear viscoelastic region, and the stress waveform is also obtained in the form of a sine wave. As mentioned before, in the linear viscoelastic region, shear stress is observed as a sinusoidal curve which is horizontally shifted by phase angle, δ, on the moment axis relative to input signal of strain. The δ depends only on angular frequency under SAOS flow. The Lissajous–Bowditch curve of Figure 1A is plotted in Figure 1B. It is an ellipse, which is characteristic of a typical Lissajous-Bowditch plot under SAOS flow. Figure 1C shows the results of FT analysis of the strain wave form in Figure 1A. Since the waveform of strain is completely sinusoidal, only the first harmonic exists but no higher harmonics in Figure 1C.

Compared with these figures, nonlinear viscoelasticity appears as a distorted strain curve as shown in Figure 1D. The Lissajous–Bowditch curve which is drawn by the wave form of Figure 1D is not elliptical. The normalized Fourier intensities of the strain curve of Figure 1D are calculated, and marked in Figure 1F. It shows strong peaks at higher odd harmonic position. As shown in Figures 1C and F, the Fourier transform is a sensitive tool to detect occurrence of nonlinearity. Even though it is hard to ascertain the nonlinear behavior from waveform of shear stress with naked eyes, the intensities of higher harmonics reveals when it starts to appear nonlinearity in stress curve. It is well known that shear stress is expressed with only odd harmonics because of its odd symmetry[29,35].

When using a stress controlled rheometer in which stress is input stimulus and strain is measured as response, the definition of compliance is required to explain the rheological behavior. According to the concrete foundation of linear viscoelastic theory, modulus and compliance can be mutually transformed with simple calculations. Bae et al. have studied based on the concern of inter–conversion relation of LAOS which are measured by the strain– and the stress–controlled rheometers[36]. Differentiation of Equation (3) in terms of time, t defines

$$\tau(t) \equiv \frac{1}{\varpi}\frac{d\sigma}{dt} = \frac{G'(\omega)}{\omega}\frac{d\gamma}{dt} - G"(\varpi)\gamma(t) \quad (6)$$

Combining Equation (3) and (6) gives

$$\gamma(t) = J'(\varpi)\sigma(t) - J"(\omega)\tau(t) \quad (7)$$
$$\frac{1}{\omega}\frac{d\gamma}{dt} = J"(\omega)\sigma(t) + J'(\omega)\tau(t)$$

where the dynamic compliance can be written as

$$J'(\omega) = \frac{G'(\omega)}{G'(\omega)^2+G''(\omega)^2};\ J''(\omega) = \frac{G''(\omega)}{G'(\omega)^2+G''(\omega)^2} \quad (8)$$

It is natural that the shear strain measured by the stress controlled rheometer satisfies

$$\gamma(-\sigma,-\tau) = -\gamma(\sigma,\tau) \quad (9)$$

The strain decomposition is also valid for LAOStress test based on its geometric characteristics[36]. It means that the shear strain changes its sign according to the direction of shear stress, σ and the rate of shear stress, τ. This is called odd symmetry. The strain signal as a response to the large amplitude oscillatory stress (LAOStress) can be expressed by the Fourier intensities as

$$\gamma(t;\sigma_o,\omega) = \sum_{k=0}^{\infty} H_{2k+1} sin[(2k+1)\varpi t + \delta_{2k+1}] \quad (10)$$

Due to the odd symmetry of the shear strain, it can be expanded by the only odd harmonics under LAOS flow. It is shown that the interference of inertia can be an obstacle for the LAOS test using stress controlled rheometer. Although it may cause the unclear scaling relation of nonlinear variables of strain decomposition, it is found that the interconversion between LAOS test of strain- and stress controlled rheometers is valid [36,37]. In order to reduce the effect of linear viscoelasticity, the relative Fourier intensity of nth order harmonics are normalized by input stress amplitude σ_0 and linear viscoelastic variable as below

$$h_n = \frac{H_n(\sigma_o,\omega)}{\sigma_o/|G^*(\omega|} \quad (11)$$

where $|G^*(\omega)| = \sqrt{G'(\omega)^2 + G''(\omega)^2}$.

In this study, the relative 3rd harmonic, h_3, of strain was used to characterize the shear flow of preconditioning step before extension step of cosmetics.

3. Experimental

3.1. Materials

It is well known that the cosmetic creams for facial care are representative viscoelastic materials. Most of cosmetic products are yield fluid, therefore it keeps its shape when the induced external stress is smaller than specific value, referred to as the yield stress. Depending on the purpose of the product, rheological properties such as viscosity, phase angle and yield stress, which are factors affecting sensory properties, are significantly changed.

Three commercial facial care creams were selected as samples, which are manufactured by E Co., L Co., and B Co.. In this study, they were named product A, product B, and product C, respectively.

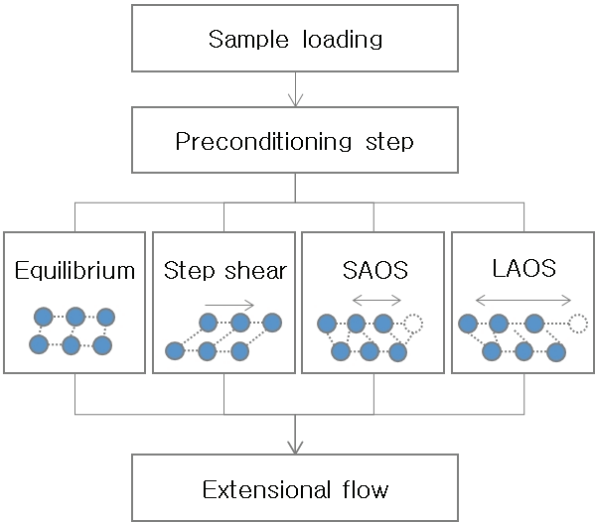

Figure 2. Flow chart of a procedure for measuring axial forces according to the different preconditioning steps: waiting for equilibrium, step shear at a constant shear rate, and oscillatory shear flow with small or large amplitudes.

3.2. Rheological Measurements

The rheological properties under various flows were measured by the stress controlled DHR3 rheometer (TA instruments, USA). All tests were performed using a 40 mm diameter geometry. In order to avoid wall slip of materials at the surface of geometry, sandblasted plate (PLASTE SST ST 40 mm SAND-BLAST ARG2, TA instruments, USA) was used. The temperature was controlled to 32 °C and the relative humidity as 45%.

The experimental procedure was designed in two steps and is summarized in the flow chart as Figure 2. The first step is preconditioning step. In this step, input deformation was induced in the sample in various ways for 60 s: (1) waiting for equilibrium without shear deformation, (2) step shear flow with constant shear rate and (3) oscillatory shear flow using small (SAOS) and (4) large amplitudes (LAOS) for 60 s. As for the oscillatory shear flow, the 3rd Fourier intensity, H_3 was calculated to understand the degree of nonlinearity in the response signal and normalized by Equation (11). The normalized H_3 was denoted h_3. In order to help understand the changes in microstructure due to the applied shear were simply expressed by circles and dashed lines. In the last step, the extensional flow was induced by lifting the upper plate vertically at a constant velocity.

The change of gap size over time was drawn in Figure 3A. Before the extensional flow, initial gap size was kept as 500 μm. At the stage of extensional flow test, the gap size increases with a constant velocity of 500 μm/s. Figure 3B shows a typical axial force curve under extensional flow as a function of time. We calculated the minimum value of axial force curve, F_{min}. The effects of preconditioning shear on F_{min} is observed in this study. All tests were repeated three times, and the mean and standard deviation were calculated to enhance the reliability of the data. Standard deviations were indicated by vertical error bars.

3.3. Texture Analyzer (TA)

The axial force curves were measured by TA on the bare skin of forearm. We introduced and used the TA measure-

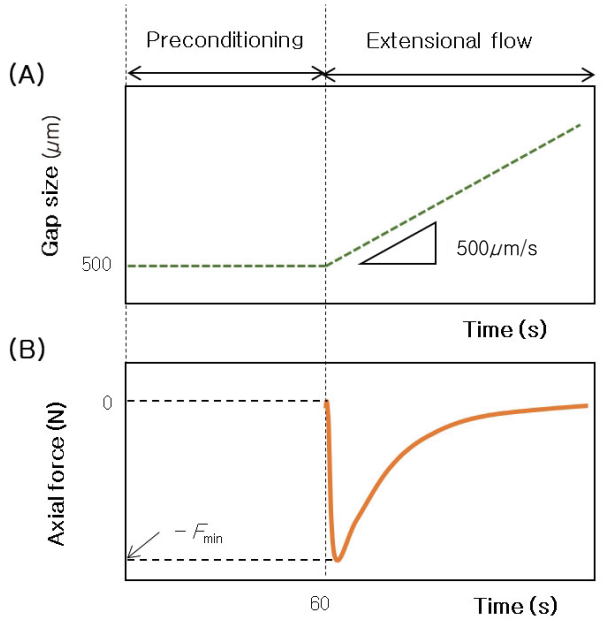

Figure 3. Schematic description of (A) gap size and (B) measured axial force curves as a function of time.

ment protocol proposed by Normandie University research group[8].

A circle with diameter of 35 mm was drawn in the middle of the forearm. The forearm skin was washed with tap water without cleansing agent. We waited more than 3 min for the skin to dry sufficiently. The 35 μL sample was loaded in a circle and spread with the forefinger for 10 s. After sample application, the waiting time was controlled as 3 min.

TA (TA XT plus, Stable Micro Systems, Cardiff, UK) was used to measure the axial force curve. A metal sphere with a diameter of 1 inch (25.4 mm) was used. The sphere facilitates pressing the substrate relatively evenly around the contact point without additional adjustment of horizontal level. The pressing speed was 1 mm/s, and the penetration depth was 10 mm from the position where the sphere came into contact with the skin. The contacted state was maintained for 2 s and the sphere returned to its initial position at a speed of 0.8 mm/s.

Figure 4 illustrates a simple form of the axial force curve that can be observe by the protocol described above. t_0 represents the time that the sphere begins to record when the

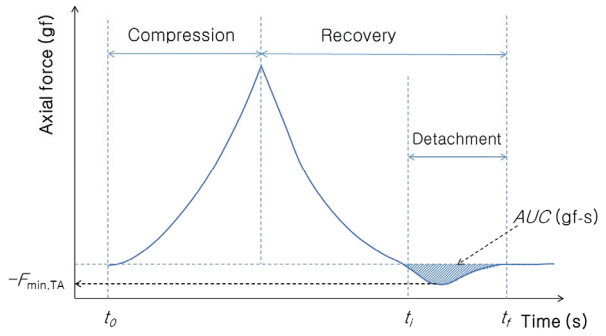

Figure 4. Simple description of axial force curve as a function of time measured by TA.

sphere touches the skin surface. t_i is the time it takes for the sphere to return to its initial position. t_f is the time it takes for the sphere to completely separate from the skin. $F_{min,TA}$ and AUC mean the minimum axial force and area under the curve, respectively.

$$AUC = -\int_{t_i}^{t_f} F(t)\,dt \tag{12}$$

where F(t) means the axial force recorded as a function of time. For convenience, AUC was defined as a positive value. $F_{min,TA}$ and AUC were calculated by Texture Exponent software. All measurements were repeated three times and data were presented through statistical analysis.

3.4. Sensory Assessment

The sensory test of stickiness for facial creams was performed by twenty volunteers aged from 20 to 40. The sensory test with volunteers was approved by the Ethical committee of LG Household & Health Care (LGHH-20200813-AA-02). The evaluation was performed for each skin without any restriction on the application method. Three samples, named with randomly assigned two-digit codes, were placed in the table. Volunteers picked the sample and applied it freely to their skin. Scores were evaluated on a 150 mm long linear scale bar. It was noted that the more sticky samples should be marked closer to the right end. The length of the scale bar from the left end was linearly converted to a score from 1 to 5. The mean value and standard deviation were calculated and marked in

figures. Difference in sensory perception between the samples were analyzed by *t*-test and the significance were marked with asterisk symbols.

4. Results and Discussion

4.1. Rheological Behaviors

The fundamental rheological properties of samples were measured by stress amplitude sweep test with ω = 1rad/s at 32 °C. Figure 5A shows the complex modulus G^* as a function of shear stress. Product C shows the highest modulus and product A shows the lowest modulus over the whole range of shear stress. Figure 5B shows the phase angle of samples. As the shear stress increase, phase angle rapidly increases after certain shear stress. The viscoelastic variables at 1 Pa were summarized in Table 1. The shear stress where G'=G" was also calculated and summarized as the cross point stress (CPS) in Table 1. When the stress amplitude of oscillatory shear flow of ω = 1rad/s exceeds CPS, G" is larger than G'. The dynamic moduli of product C are the highest value compared to other samples. According to phase angle, δ, product C exhibits a relatively liquid-like behavior compared to products A and B, while product A exhibits a relatively elastic behavior in the entire sample.

Figure 6A shows the storage and loss moduli of product

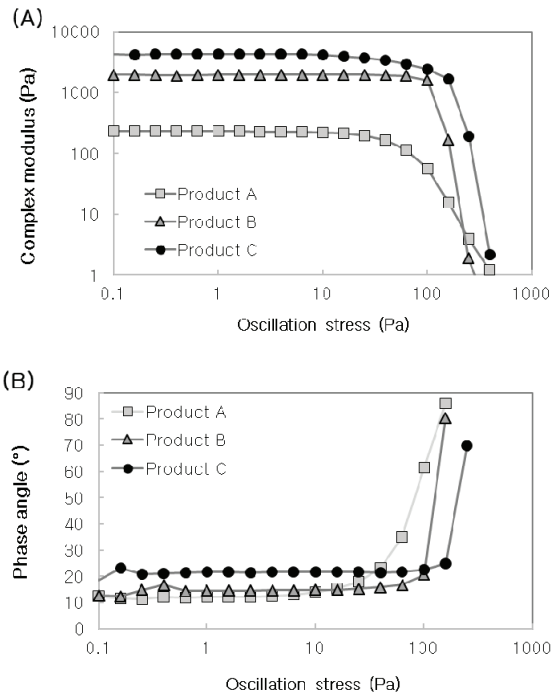

Figure 5. (A) Complex modulus and (B) phase angle as a function of shear stress under oscillatory shear flow with ω = 1 rad/s.

Table 1. Viscoelastic Variables under Oscillatory Shear of σ = 1 Pa and ω = 1 rad/s

Viscoelastic variables	G' (Pa)	G" (Pa)	G* (Pa)	δ (°)	CPS (Pa)
Product A	224.6	48.01	229.6	12.07	74.92
Product B	1891	490.4	1954	14.54	117.8
Product C	3986	1572	4285	21.53	193.3

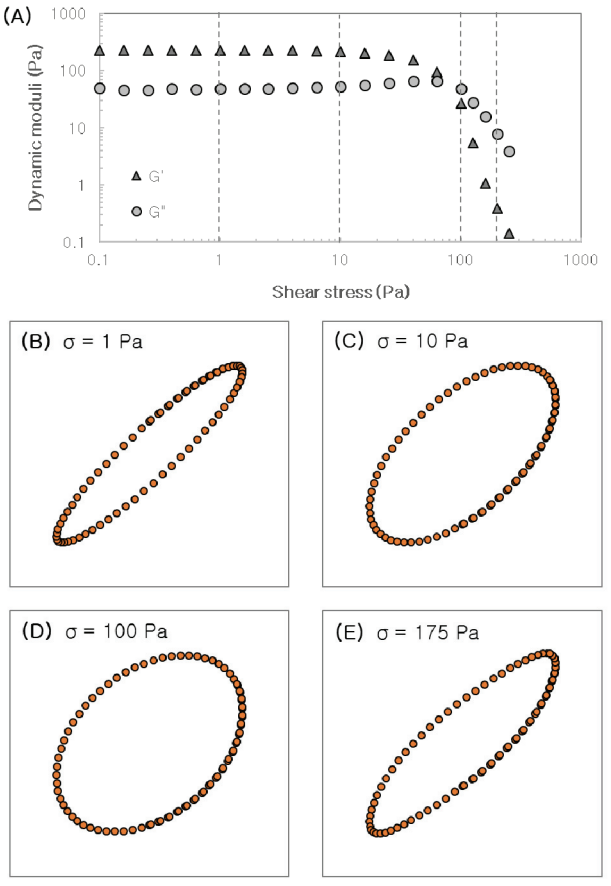

Figure 6. (A) Storage and Loss moduli of product A as a function of shear stress. The Lissajous-Bowditch plots is plotted by the normalized strain versus the normalized stress at (B) 1 Pa, (C) 10 Pa, (D) 100 Pa and (E) 175 Pa.

A as a function of shear stress. At the shear stress marked with dashed vertical lines in Figure 6A, the Lissajous-Bowditch plots were plotted in Figure 6B ~ E using normalized stress as the x-axis and normalized strain as the y-axis. When the shear stress are 1 Pa and 10 Pa, Figure 6B and 6C show the elliptic curves due to the linear relation between input stress and output strain. When the shear stress is 100 Pa (Figure 6D), it is hard to figure out whether the curve is completely elliptical or not. At 175 Pa of shear stress, it is clear that the Lissajous-Bowditch plot is distorted from the elliptic curve. As mentioned above, the Lissajous-Bowditch plot can simply visualize the linear and nonlinear relation between input and output signals. However, it is difficult to quantitatively characterize the nonlinearity of the signal. Hence, we used the relative Fourier intensity of the 3rd harmonic (h_3) to compare the effects of oscillatory flow in the preconditioning step.

4.2. Effects of Preconditioning Shear Flow on the Axial Force

The axial force under extensional flow were plotted in Figure 7. For clarity, curves are vertically shifted with the arbitrary shifting factor, α. As the gap between the Peltier and the upper plate increases, the axial force is recorded in a timely manner, and the value is negative due to its direction. In this study, we considered only the axial force not normal stress, because the area change on the perpendicular plane to the extensional direction was not recorded. At a certain time, the axial force reached to the global minimum and increased as gap size increased. The global minimum value was calculated as F_{min}. It is interesting that the local minimum were observed for all samples. According to the previous research using TA, it was reported that inhomogeneity of micro gel structure causes occurrence of local minimum in the axial force curves under extensional flow using TA[6].

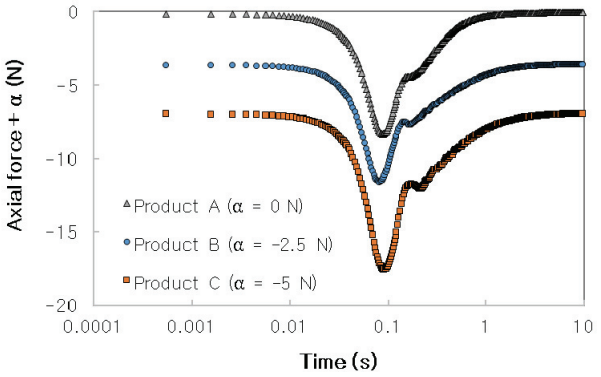

Figure 7. Axial force as a function of time at the stage of extensional flow. The curves are vertically shifted by arbitrary shift factors, α.

F_{min} obtained from the axial force curves were summarized in Table 2 for 3 samples according to the different preconditioning steps. When no shear flow was induced at the stage of preconditioning step, F_{min} of samples were sim-

Table 2. F_{min} of Samples according to Different Preconditioning Steps

Sample	Equilibrium (No shear)	Step shear	Osillatory shear (ω = 1 rad/s)			
			1 Pa	10 Pa	100 Pa	1,000 %
Product A	9.52	7.62	9.82	9.66	9.37	8.50
Product B	13.11	7.68	12.59	12.35	9.11	8.13
Product C	22.35	5.86	19.02	18.42	18.32	12.58

Table 3. Parameters of Empirical Equation (13) for F_{min}

	F_0 (N)	h_0 (-)	n (-)	r^2 (-)
Product A	10.01	4.57	0.3356	0.997
Product B	12.52	0.5186	0.6114	0.994
Product C	18.66	0.7944	0.7794	0.995

ilar to the results which are measured after SAOS flow (1 Pa and 10 Pa). It means that the SAOS flow induced in the preconditioning step barely leads to the deformation of microstructure. As for the product C, F_{min} dramatically decreased after the step shear with a constant shear rate, 1 rad/s. The step shear increases the strain over time because it constantly applies shear flow. Hence, the step shear flow is an experimental method that greatly deforms the microstructure of material. This phenomenon is especially common in viscoelastic materials with high modulus. For this reason, the step shear flow is difficult to keep the loaded sample stable during rotation. This is one of the reasons that LAOS flow attracts attention as a tool to investigate the nonlinear behavior of viscoelastic materials. When the large amplitude oscillatory stress (100 Pa) and large amplitude oscillatory strain (1,000%) were induced before the extension test, relative tendency of F_{min} of each samples are similarly observed. According to Figure 5, oscillatory amplitude 100 Pa is higher than CPS for product A but not for product B and C. It means that the flow derived by a fixed stress amplitude can be either a SAOS (linear deformation) or a LAOS (nonlinear deformation) flow depending on the material. In other words, the fixed stress amplitude can be an ambiguous boundary as a preconditioning shear condition.

In order to characterize the oscillatory shear flows as an input signal, the 3rd Fourier intensities H_3 was calculated by the harmonic analysis function of TRIOS software (TA instruments, USA). Subsequently, h_3 was calculated by normalization using linear viscoelastic variable as defined in Equation (11). The h_3 and F_{min} of product A were plotted as a function of shear stress in Figure 8A. As shear stress increases, F_{min} measured after oscillatory shear flow decreased as shown in Table 2. h_3 is nearly 0 when the oscil-

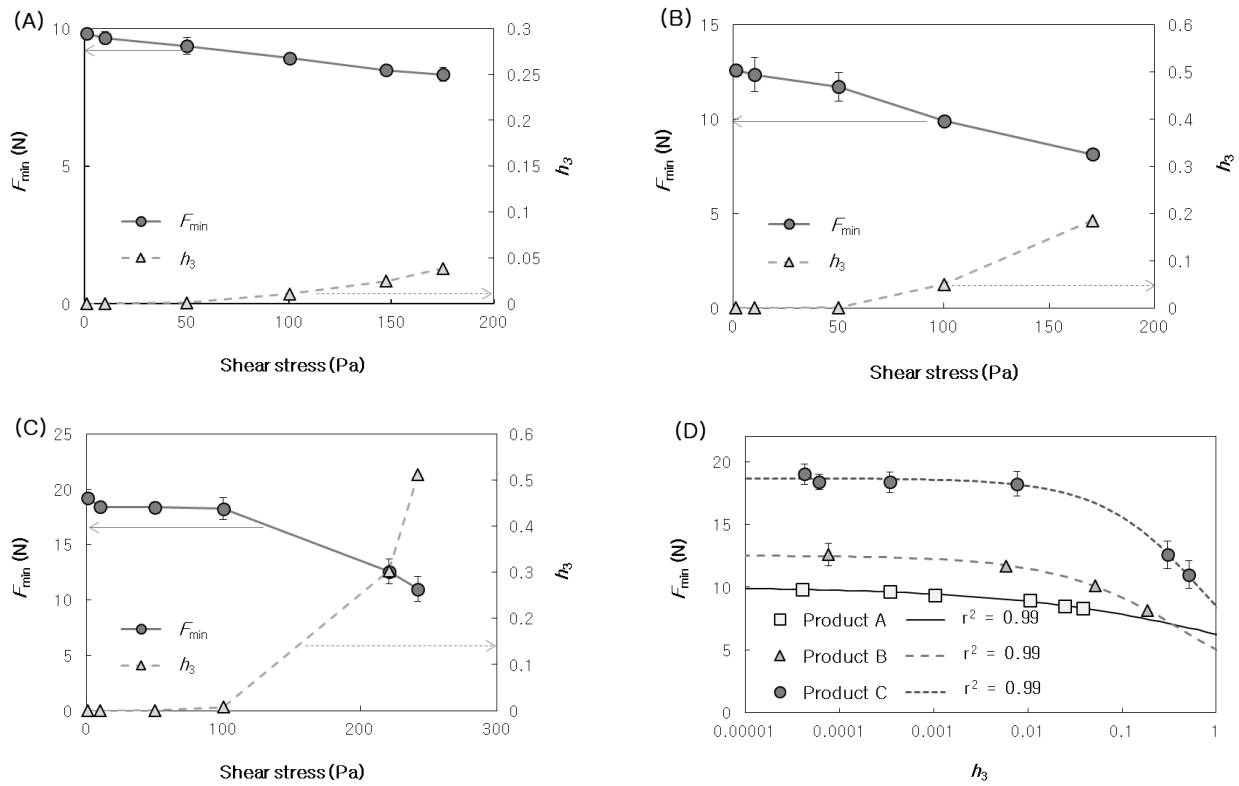

Figure 8. F_{min} and h_3 as a function of shear stress for (A) product A, (B) product B; (C) product C. (D) F_{min} and empirical equations as functions of h_3 for all samples. Symbols are data measured by rotational rheometer. Solid, dashed, and dotted lines represent predictions based on empirical equations.

latory stress is below 50 Pa. As shear stress increases over 50 Pa, h_3 also increases. It means that the response strain signal starts to show nonlinearity and the input stress causes changes in microstructures. Figure 8B∼C show h_3 and F_{min} as a function of shear stress of products B and C, respectively. As for the result of product B, h_3 was 5.2 x 10^{-2} when the oscillatory stress amplitude was 100 Pa, while h_3 of product C was 7.7 x 10^{-3} even if the same stress amplitude (100 Pa) was induced to the samples. When the input signal with same amplitude is applied, whether the strain output is linear or nonlinear depends on the properties of the material.

Symbols in Figure 8D show the relation between F_{min} and h_3. If h_3 is almost zero, especially below 0.01, F_{min} remains similar regardless of h_3. When a sufficiently large amplitude oscillatory flow was induced in the samples, h_3 increased while F_{min} decreased.

In order to compare the effects of nonlinear deformation on F_{min} of each sample, the empirical equation is suggested as below:

$$F_{\min}(h_3) = \frac{F_0}{1+\left({h_3}/{h_0}\right)^n} \quad (13)$$

The nonlinear regression yields parameters describing F_{min} of each sample with a high accuracy of $r^2 > 0.99$, where r^2 is the coefficient of determination. The parameters were summarized in Table 3. When h_3 is approximated to 0, F_{min} corresponds to F_0. It is expected that F_0 are related to linear viscoelastic variables under SAOS flow. In equation (13), n is related to the slope of decreasing F_{min} as h_3 increases. According to the parameter obtained by regression, n of product C was largest, and F_{min} of that sharply decreased as nonlinearity of deformation increased. By solving the system of equation numerically, an intersection of F_{min} curves of products A and B appears where h_3 = 0.34.

The process of spreading cosmetics on the skin is a process accompanied by significant deformation of microstructures. Various methods have been proposed to simulate these steps using mechanical devices and to investigate rheological behavior. However, the measurement of rheological properties using step shear with large deformation has experimental problems such as low reproducibility and unstable loading conditions. In this respect, unlike other flows, LAOS flow is a suitable way to stably measure nonlinearity while using large deformations. SAOS flow with h_3 of 0.01 or less does not cause sufficient deformation of the material, so it exhibits a behavior similar to the measured axial force without applying preconditioning shear. After applying LAOS flow showing a sufficiently large h_3, the axial force tends to differ from the effect of the preconditioning step using no shear or SAOS flow.

4.3. Comparison with Axial Force Measured by Texture Analyzer

The axial force curves were measured as described in Figure 4 and the tests were repeated in three times. Figure 9 shows the results of TA measurements and sensory evaluation. Product C has the largest $F_{min,TA}$, while product A has the smallest value. Standard deviations were indicated by vertical error bars. According to statistical analysis of the results, products A and B did not show the significant difference. The not significant difference was also observed between the results of products B and C. On the other hand, products A and C showed significant difference

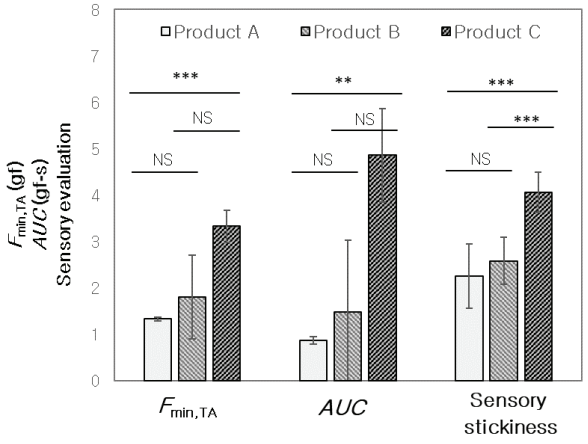

Figure 9. Comparison of statistical analysis of $F_{min,TA}$, AUC measured by TA and sensory assessment for stickiness by panel test. NS: non-significant, $^{*}p < 0.05$, $^{**}p < 0.01$, $^{***}p < 0.001$

with $p < 0.001$. The *AUC* trend of all samples was similar to that of $F_{min,TA}$.

It is interesting that the panel test shows a significant difference compared to the TA results. Through panel test, product C scored the highest score on stickiness and it showed significant difference with not only products A but also B.

Based on the results of panel test and the empirical equations of F_{min}, it is expected that shear deformation of $h_3 \approx 0.34$ will be required to measure the stickiness of the samples concerned in this study.

5. Conclusions

The texture of cosmetics is one of the most important factors determining the quality of products. In order to investigate the effect of mechanical properties on sensory properties, various methods have been suggested to quantitatively measure the sensory properties.

The method of measuring the axial force using TA has been continuously studied until recently to find a correlation with stickiness. It was found that the axial force measured by TA on the skin covered by cosmetics has a positive correlation with the stickiness evaluated by panel test[8]. Although they investigated the effects of substrate and suggested the most suitable conditions for accurate measurements, it still suffers from the weak reproducibility due to differences in spreading conditions of samples.

In this study, we suggested a new procedure to measure the axial force under extensional flow using a rotational rheometer. The procedure consists of 3 steps: sample loading step, preconditioning step and extension step. At the preconditioning step, linear and nonlinear shear deformation were induced using step shear, SAOS and LAOS flow, and the effects of preconditioning shear on the axial force at the extension step were observed. It is found that the axial force, which is expected to be related to the sensory stickiness, is affected by the preconditioning flow step. As for the step shear, it leads to significant deformation to the samples, but it is hard to obtain the proper measured data due to unstable loading state during rotation. When the SAOS flow is induced to the samples, F_{min} was measured as similar as that measured without pre-shear conditioning. It means that SAOS flow cannot lead the sufficient deformation on the microstructure of samples.

Compared with SAOS, the LAOS flow as a preconditioned flow resulted in different consequences of axial forces in the expansion step. It is important to characterize the nonlinearity of LAOS flow at the preconditioning step, because even if the same stress amplitude is applied, nonlinear deformation may or may not occur depending on the materials. Nonlinear viscoelastic flow is characterized by the normalized 3rd Fourier intensity, h_3, and the F_{min} observed as a function of h_3. According to the samples, the dependence of nonlinearity of shear deformation at preconditioning step was differently observed. The empirical equations were simply suggested to quantitatively compare the axial force behavior as a function of h_3.

Axial forces measured by rheometer were compared with those by TA and results of panel test. It is found that the TA test provided the axial force data similar to that measured by a rotational rheometer, but it has few statistically significant differences. It is shown that shear deformation with $h_3 \approx 0.34$ is required to describe the stickiness scored by the panel test using a rotational rheometer with high reproducibility as well as significant differences.

It is worth noting that the h_3 can be a criterion determining the amplitude of oscillatory shear to design the procedure measuring the axial force related to the stickiness of cosmetics. A suitable protocol for measuring the stickiness of the cream should be accompanied by a pretreatment shear with a sufficiently large amplitude, which is likely to reflect changes in the microstructure while applying the cream to the skin. It is expected that the newly suggested protocol using h_3 parameter enables the evaluation of the stickiness of cosmetics in a more systematic way.

References

1. L. S. Calixto, P. M. B. G. M. Campos, C. Picard, and G. Savary, Brazilian and French sensory perception of complex cosmetic formulations: a cross-cultural study,

Int. J. Cosmet. Sci., **42**(1), 60 (2020).
2. K. Timm, C. Myant, H. Nuguid, H. A. Spikes, and M. Grunze, Investigation of friction and perceived skin feel after application of suspensions of various cosmetic powders, *Int. J. Cosmet. Sci.*, **34**(5), 458 (2012).
3. K. Kusakari, M. Yoshida, F. Matsuzaki, T. Yanaki, H. Fukui, and M. Date, Evaluation of post-application rheological changes in cosmetics using a novel measuring device: relationship to sensory evaluation, *J Cosmet Sci*, **54**(4), 321 (2003).
4. K. Nakano, K. Kobayashi, K. Nakao, R. Tsuchiya, and Y. Nagai, Tribological method to objectify similarity of vague tactile sensations experienced during application of liquid cosmetic foundations, *Tribol. Int.*, **63**, 8 (2013).
5. E. Gore, C. Picard, and G. Savary, Complementary approaches to understand the spreading behavior on skin of O/W emulsions containing different emollients, *Colloids Surf. B*, **193**, 111132 (2020).
6. A. Tai, R. Bianchini, and J. Jachowicz, Texture analysis of cosmetic-pharmaceutical raw materials and formulations, *Int. J. Cosmet. Sci.*, **36**(4), 291 (2014).
7. M. Lukic, I. Jaksic, V. Krstonosic, N. Cekicà, and S. Savic, A combined approach in characterization of an effective w/o hand cream: the influence of emollient on textural, sensorial and *in vivo* skin performance, *Int. J. Cosmet. Sci.*, **34**(2), 140 (2012).
8. F. Eudier, D. Hirel, M. Grisel, C. Picard, and G. Savary, Prediction of residual film perception of cosmetic products using an instrumental method and non-biological surfaces: the example of stickiness after skin application, *Colloids Surf. B*, **174**, 181 (2019).
9. J. L¨auger and H. Stettin, Differences between stress and strain control in the non-linear behavior of complex fluids, *Rheol. Acta,* **49**, 909 (2010).
10. K. Suzuki and T. Watanabe, Relationship between sensory assessment and rheological properties of cosmetic creams, *J. Texture Stud.*, **2**(4), 431 (1971).
11. A. Z. Nelson and R. H. Ewoldt, Design of yield-stress fluids: a rheology-to-structure inverse problem, *Soft matter*, **13**, 7578 (2017).
12. G. Tafuro, A. Costantini, G. Baratto, L. Busata, and A. Semenzato, Rheological and textural characterization of acrylic polymer water dispersions for cosmetic use, *Ind. Eng. Chem. Res.*, **58**, 23549 (2019).
13. S. Ozkan, T. W. Gillece, L. Senak and D. J. Moore, Characterization of yield stress and slip behavior of skin/hair care gels using steady flow and LAOS measurements and their correlation with sensorial attributes, *Int. J. Cosm. Sci.*, **34**(2), 193 (2012).
14. A. Zosel, Adhesive failure and deformation behavior of polymers, *J. Adhes.*, **30**, 135 (1989).
15. B. J. Dobraszczyk, The rheological basis of dough stickiness, *J. Texture Stud.,* **28**, 139 (1997).
16. Z. Yuan, J. Wang, X. Niu, J. Ma, X. Qin, L. Li, L. Shi, Y. Wu, and X. Guo, A study of the surface adhesion and rheology properties of cationic conditioning polymers, *Ind. Eng. Chem. Res.*, **58**(22), 9390 (2019).
17. B. Andreotti and J. H. Snoeijer, Statics and dynamics of soft wetting, *Annu. Rev. Fluid Mech.*, **52**, 285 (2020).
18. N. Baït, C. Derail, A. Benaboura, and B. Grassl, Rheology and adhesive properties versus structure of poly(acrylamide-co-hydroxyethyl methacrylate) hydrogels, *Int. J. Adhes. Adhes.*, **96**, 102449 (2020).
19. H. M. Laun and J. Meissner, A sandwich-type creep rheometer for the measurement of rheological properties of polymer melts at low shear stress, *Rheol. Acta*, **19**, 60 (1980).
20. W. Philippoff, Vibrational measurements with large amplitudes, *Trans. Soc. Rheol.*, **10**, 317 (1966).
21. A. T. Tsai and D. S. Soong, Measurement of fast transient and steady state responses of viscoelastic fluids with sliding cylinder rheometer executing coaxial displacements, *J. Rheol.*, **29**, 1 (1985).
22. T. B. Goudoulas and N. Germann, Concentration effect on the nonlinear measures of dense polyethylene oxide solutions under large amplitude oscillatory shear, *J. Rheol.*, **62**, 1299 (2018).
23. A. J. Giacomin, R. S. Jeyaseelan, T. Samurkas, and

J. M. Dealy, Validity of separable BKZ model for large amplitude oscillatory shear, *J. Rheol.*, **37**, 811 (1993).
24. H. M. Laun, Prediction of elastic strains of polymer melts in shear and elongation, *J. Rheol.*, **30**, 459 (1986).
25. F. J. Stadler, A. Leygue, H. Burhin, and C. Bailly, The potential of large amplitude oscillatory shear to gain an insight into the long-chain branching structure of polymers, Proceeding of the 235th ACS National Meeting, *polymer preprints ACS*, **49**, 121, New Orleans, LA, USA (2008).
26. J. E. Bae and K. S. Cho, Semianalytical methods for the determination of the nonlinear parameter of nonlinear viscoelastic constitutive equations from LAOS data, *J. Rheol.*, **59**, 525 (2015).
27. R. S. Jeyaseelan and A. J. Giacomin, Network theory for polymer solutions in large amplitude oscillatory shear, *J. Nonnewton. Fluid Mech.*, **148**, 24 (2008).
28. R. H. Ewoldt and G. H. McKinley, On secondary loops in LAOS via self–intersection of Lissajous–Bowditch curves, *Rheol. Acta*, **49**, 213 (2010).
29. K. S. Cho, K. Hyun, K. H. Ahn, and S. J. Lee, A geometrical interpretations of large amplitude oscillatory shear response, *J. Rheol.*, **47,** 747 (2005).
30. S. A. Rogers and M. P. Lettinga, A sequence of physical processes determined and quantified in LAOS: application to theoretical nonlinear models, *J. Rheol.*, **56**, 1 (2012).
31. C. R. López–Barrón, N. J. Wagner, and L. Porcar, Layering, melting, and recrystallization of a close–packed micellar crystal under steady and large–amplitude oscillatory shear flows, *J. Rheol.*, **59**, 793 (2015).
32. M. Wilhelm, D. Maring, and H. W. Spiess, Fourier–transform Rheology, *Rheol. Acta*, **37**, 399 (1998).
33. M. Wilhelm, P. Reinheimer, and M. Ortseifer, High sensitivity Fourier-transform rheology, *Rheol. Acta*, **38**, 349 (1999).
34. T. Neidhofer, M. Wilhelm, and B. Debbaut, Fourier-transform rheology experiments and finite-element simulations on linear polystyrene solutions, *J. Rheol.*, **47**, 1351 (2003).
35. R. H. Ewoldt, A. E. Hosoi, and G. H. McKinley, New measures for characterizing nonlinear viscoelasticity in large amplitude oscillatory shear, *J. Rheol.*, **52,** 1427 (2008).
36. J. E. Bae, M. Lee, K. S. Cho, K. H. Seo, and D. G. Kang, Comparison of stress-controlled and strain-controlled rheometers for large amplitude oscillatory shear, *Rheol. Acta*, **52**, 841 (2013).
37. K. S. Cho, K. W. Song, and G. S. Chang, Scaling relations in nonlinear viscoelastic behavior of aqueous PEO solutions under large amplitude oscillatory shear flow, *J. Rheol.,* **54**, 27 (2010).

Supplementary Materials

In order to verify the reproducibility of protocol to measure the axial force, an aqueous solution of commercial polymer was selected and the axial force was measured by a rotational rheometer and TA. The results of the rheometer and TA are summarized in Tables S1 and S2, respectively. The polymer was Carbopol® 980 supplied by Lubrizol. The solution contains 0.5% Carbopol® as neutralized form and 2% of 1,2-hexandiol as preservative. All test were repeated three times and the mean and standard deviation were calculated.

Table S1. F_{min} of 0.5% Carbopol® 980 Aqueous Solution

	Equilibrium	Step shear	Oscillatory shear (ω = 1 rad/s)			
			1 Pa	10 Pa	100 Pa	1,000 %
F_{min} (N)	9.762	9.079	9.159	9.054	8.722	9.079
Standard deviation (N)	0.4198	0.01905	0.4574	0.4303	0.4013	0.01906
h_3 (-)			5.084×10^{-5}	1.601×10^{-4}	1.280×10^{-1}	6.212

Table S2. $F_{min,TA}$ and AUC of 0.5% Aqueous Carbopol® 980 Solution

	Average	Standard deviation
$F_{min,TA}$ (g_f)	1.5	0.1
AUC ($g_f \cdot s$)	1.039	9.613×10^{-2}